

# Effects of Short-Axis Alkoxy Substituents on Molecular Self-Assembly and Photovoltaic Performance of Indacenodithiophene-Based Acceptors

Xiaojun Li, He Huang, Indunil Angunawela, Jiadong Zhou, Jiaqi Du, Alex Liebman-Pelaez, Chenhui Zhu, Zhanjun Zhang, Lei Meng, Zengqi Xie,\* Harald Ade,\* and Yongfang Li\*

The effects of central alkoxy side chain length of a series of narrow bandgap small molecule acceptors (SMAs) on their physicochemical properties and on the photovoltaic performance of the SMA-based polymer solar cells (PSCs) are systematically investigated. It is found that the ordered aggregation of these SMAs in films is enhanced gradually with the increase of alkoxy chain length. The single-crystal structures of these SMAs further reveal that small changes in the side chain length can have a dramatic impact on molecular self-assembly. The short-circuit current density and power conversion efficiency values of the corresponding PSCs increase with the increase of the side chain length of the SMAs. The  $\pi-\pi$  coherence length of the SMAs in the active layers is increased with the increase of the side chain length, which could be the reason for the increase of the  $J_{sc}$  in the PSCs. The results indicate that small changes in side chain length can have a dramatic impact on the molecular self-assembly, morphology, and photovoltaic performance of the PSCs. The structure–performance relationship established in this study can provide important instructions for the side chain engineering and for the design of efficient SMAs materials.

## 1. Introduction

Polymer solar cells (PSCs) are considered as a promising next-generation green technology for energy sources, owing to their

low cost, light weight, and flexibility.<sup>[1–6]</sup> Since 2015, the power conversion efficiency (PCE) of single-junction PSCs has increased from ≈10% to 15–16%.<sup>[7–10]</sup> The breakthrough of the PCE values in recent years is greatly benefitted from the development of the low bandgap acceptor-donor-acceptor (A-D-A)-structured small molecule acceptors (SMAs). However, the reasons behind the success of the A-D-A SMAs are complicated, the relationships between structure, molecular packing, donor-acceptor interface and phase separation are still vague. Considering that these relationships are reliant upon subtle changes of molecular structure and significantly affect the intermolecular electronic interactions, charge-transfer states and ultimately device performance. The detailed study on underlying working mechanism from the perspective of chemical structures of the SMAs became crucially important, which will benefit the design of efficient photovoltaic materials and promote the improvement of the device performance.

In the A-D-A structured SMAs, there are three main components in their chemical structures: central fused ring donor (D)

Dr. X. Li, J. Du, Prof. L. Meng, Prof. Y. Li  
Beijing National Laboratory for Molecular Sciences  
CAS Key Laboratory of Organic Solids  
Institute of Chemistry  
Chinese Academy of Sciences  
Beijing 100190, China  
E-mail: liyf@iccas.ac.cn

Dr. X. Li, H. Huang, J. Du, Prof. Z. Zhang, Prof. Y. Li  
School of Chemical Science  
University of Chinese Academy of Sciences  
Beijing 100049, China  
Dr. I. Angunawela, Prof. H. Ade  
Department of Physics and Organic and Carbon Electronics Lab (ORaCEL)  
North Carolina State University  
Raleigh, NC 27695, USA  
E-mail: hwade@ncsu.edu

Dr. J. Zhou, Prof. Z. Xie  
Institute of Polymer Optoelectronic Materials and Devices  
State Key Laboratory of Luminescent Materials and Devices  
South China University of Technology  
Guangzhou 510640, China  
E-mail: msxiez@scut.edu.cn  
Dr. A. Liebman-Pelaez, Dr. C. Zhu  
Advanced Light Source  
Lawrence Berkeley National Laboratory  
Berkeley, CA 94720, USA  
Prof. Y. Li  
Laboratory of Advanced Optoelectronic Materials  
College of Chemistry  
Chemical Engineering and Materials Science  
Soochow University  
Suzhou, Jiangsu 215123, China

 The ORCID identification number(s) for the author(s) of this article can be found under <https://doi.org/10.1002/adfm.201906855>.

DOI: 10.1002/adfm.201906855

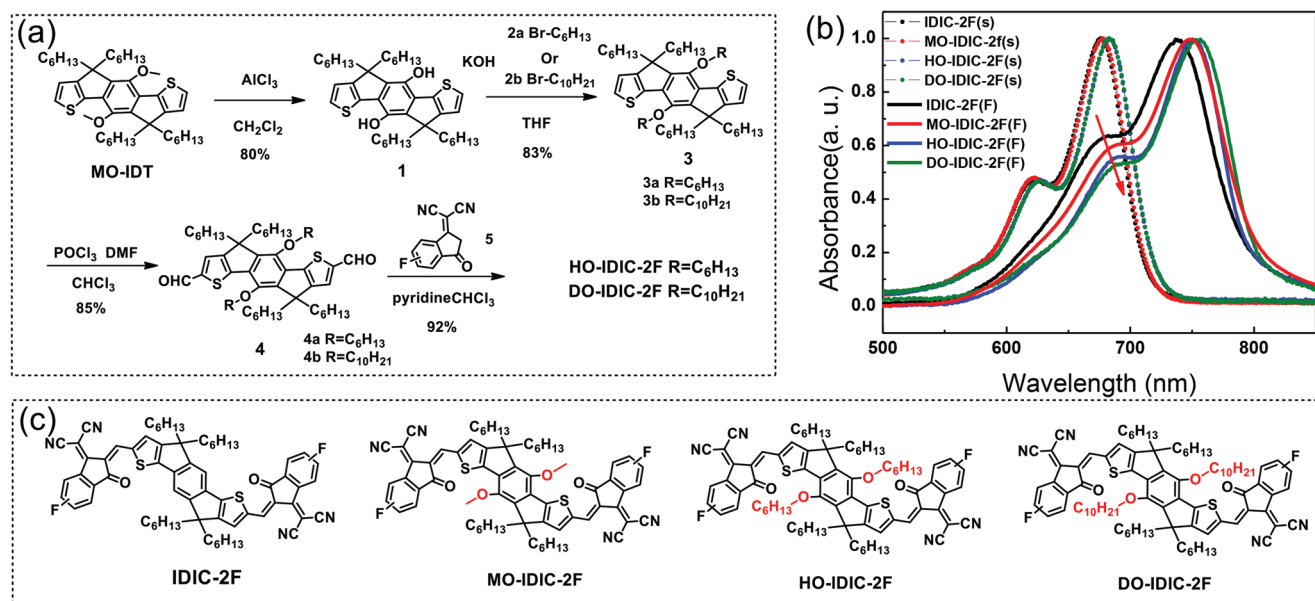


**Figure 1.** a) Synthetic routes of HO-IDIC-2F and DO-IDIC-2F. b) Absorption spectra of IDIC-2F, MO-IDIC-2F, HO-IDIC-2F, and DO-IDIC-2F in chloroform solutions (S) and films state (F), c) Chemical structures of IDIC-2F, MO-IDIC-2F, HO-IDIC-2F, and DO-IDIC-2F.

unit, electron-withdrawing (A) end-caps and side chains on the central fused ring.<sup>[11,12]</sup> The absorption spectra and electronic energy levels of the SMAs can be tuned effectively by using different D- and A-units.<sup>[13–18]</sup> While the side chains can regulate solubility and intermolecular packing of the SMAs, which further influence the nanoscale or mesoscale morphology and charge transport properties of the BHJ photoactive layers.<sup>[19–25]</sup> Moreover, the difference in morphology of the blend films will ultimately affect the PCE of the PSCs.

In recent years, many groups have performed a lot of research on the influence of side chains on molecular self-aggregation and morphology of the active layers. For instance, Heeney and co-workers reported C8-ITIC, comparison of its properties to ITIC, the alkylation results in a reduced optical bandgap and an increased crystallinity.<sup>[26]</sup> Bo and co-workers reported a new SMA IDT-OB with aryl and alkyl side chains, which exhibit obviously decreased crystallinity compared to alkyl-substituted IDT-2O. As a result, the blend active layer based on IDT-OB possesses better morphology than that of IDT-2O with strong aggregation and large domains.<sup>[19]</sup> Yang et al. reported the IDIC-C4Ph and provided an effective approach via side chain modification to modulate the aggregation and morphology of the acceptors.<sup>[20]</sup> Our group reported *m*-ITIC with *m*-hexylphenyl as side chains, compared with its isomeric counterpart ITIC, *m*-ITIC shows a larger crystalline coherence.<sup>[27]</sup> Furthermore, we investigated the effects of side chain regiochemistry on the self-assembly and active layer morphology of the SMAs TPTC and TPTIC.<sup>[28]</sup> Despite of these studies, the information about the effect of side chains on the self-assembly properties of the SMAs are still limited, the intrinsic causes of morphological differences are ambiguous and the correlation between properties and molecular structures need to be further elucidated.

Here, we synthesized two new SMAs of HO-IDIC-2F and DO-IDIC-2F, and studied the effect of side chain engineering

of the SMAs on the physicochemical, self-assembly and photovoltaic properties of a series of SMAs: IDIC-2F, MO-IDIC-2F, HO-IDIC-2F, and DO-IDIC-2F (Figure 1c), with different alkoxy substituents in the central fused ring donor units. We found that the absorption spectra red-shifted and the lowest unoccupied molecular orbital (LUMO) up-shifted gradually with the increase of alkyl chain length of the side chains from IDIC-2F to DO-IDIC-2F. In addition, the single-crystal analysis, computed intermolecular interaction energies and grazing incidence wide-angle X-ray scattering (GIWAXS) measurement in thin films indicate that small side chain variation yields vastly different molecular self-assembly. PCE values of the PSCs based on the SMAs with PM6 as donor were improved with the increase of the alkoxy chain length of the SMAs from 11.52% for the IDIC-2F-based PSCs to 13.02% for the DO-IDIC-2F-based PSCs. Furthermore, GIWAXS experiment of blend films provide insights about the changes in the morphology of photoactive layers based on these SMAs. The analysis based on this class of SMAs may contribute to the fundamental understanding of the role of side chains and establish the connection between side chain structures, chemical properties, molecular self-assembly, blend film morphology and the PCE of the devices.

## 2. Synthesis of HO-IDIC-2F and DO-IDIC-2F

Compound IDIC-2F and MO-IDIC-2F were synthesized according to our previous publication<sup>[29]</sup> and the synthetic routes of HO-IDIC-2F and DO-IDIC-2F are shown in Figure 1a. The detailed synthetic procedures of HO-IDIC-2F and DO-IDIC-2F are described in the Supporting Information. Compound MO-IDT was synthesized according to our previous publication.<sup>[29]</sup> Intermediate 1 was prepared by demethylation reaction

of MO-IDT using  $\text{AlCl}_3$  as catalyst at room temperature. Then crude product 1 was dissolved in dry THF and then reacted with compound 2. After being stirred at reflux condition for 24 h, the compound 3 was obtained using column chromatography on silica gel employing petroleum ether/ $\text{CH}_2\text{Cl}_2$  (1:6) as an eluent. Then the intermediate 4 was prepared by Vilsmeier–Haack reaction of 3 with  $\text{POCl}_3$  in DMF. Subsequently, target molecules HO-IDIC-2F and DO-IDIC-2F were synthesized by Knoevenagel condensation of 4 with compound 5 in high yield (92% for HO-IDIC-2F and 89% for DO-IDIC-2F) as dark blue solids. The chemical structure of each new compound is fully characterized by  $^1\text{H}$  NMR,  $^{13}\text{C}$  NMR, and MALDI-TOF. And the  $^1\text{H}$  NMR,  $^{13}\text{C}$  NMR, and high resolution mass spectrometry (HRMS) spectra of HO-IDIC-2F and DO-IDIC-2F were shown in Figures S1–S6 in the Supporting Information. The thermal stability of these two compounds was investigated using thermo gravimetric analysis (TGA) under nitrogen atmosphere (Figure S7, Supporting Information). The TGA curves of HO-IDIC-2F and DO-IDIC-2F show decomposition temperatures ( $T_d$ , 5% weight loss) of 334 and 331 °C, respectively, which indicates both of them have good thermal stability for the application as photovoltaic materials in PSCs.

As shown in Figure 1c, these four SMAs of IDIC-2F, MO-IDIC-2F, HO-IDIC-2F, and DO-IDIC-2F have the same  $\pi$ -conjugated backbone and only differ in the alkoxy chains attached to the central benzene ring of their fused ring donor unit. Specifically, the alkyl chain length of the alkoxy side chains increases from IDIC-2F without alkoxy substituent to DO-IDIC-2F with decyloxy substituents. In the following, we studied the effect of the alkoxy side chains length on the physicochemical, self-assembly, and photovoltaic properties of the four SMAs.

### 3. Absorption Spectra and Electronic Energy Levels

Figure 1b shows the UV-vis absorption spectra of IDIC-2F, MO-IDIC-2F, HO-IDIC-2F, and DO-IDIC-2F in solutions and films. In solutions, these SMAs exhibited similar absorption range from 550 to 730 nm, and HO-IDIC-2F and DO-IDIC-2F with longer alkyl chains have slightly red-shifted absorption than the other acceptors. In films, all the SMAs exhibit red-shifted absorption in comparison with their solutions, which could be attributed to their ordered aggregation in films, and the absorption spectra of the SMAs redshift gradually with the increase of alkoxy chains lengths from IDIC-2F to DO-IDIC-2F. The maximum absorption ( $\lambda_{\max}$ ) of the four SMAs are at 722, 735, 739, and 744 nm, with optical bandgaps ( $E_g^{\text{opt}}$ ) of 1.57, 1.55, 1.55, and 1.54 eV for IDIC-2F, MO-IDIC-2F, HO-IDIC-2F, and DO-IDIC-2F, respectively. In addition, these SMAs show obvious shoulder peaks at around 650–660 nm. The intensity of the shoulder peaks at  $\approx$ 660 nm are distinctly decreased as the alkoxy chains lengths increase, indicating the side-chain dependence of intramolecular aggregation property of these SMAs.<sup>[30,31]</sup> And from IDIC-2F to DO-IDIC-2F, the decreased intensity of the shoulders elucidated a gradually enhanced aggregation feature, and the most ordered molecular arrangement will be beneficial to the more efficient charge transport.

Electronic energy levels of these SMAs were measured by electrochemical cyclic voltammetry with Ag/AgCl as reference

**Table 1.** Physicochemical properties and electronic energy levels of the SMAs.

	$\lambda_{\max}^{\text{a)}$ [nm]	$\lambda_{\text{edge}}^{\text{a)}$ [nm]	$E_g^{\text{optb)}$ [eV]	$E_{\text{HOMO}}^{\text{c)}$ [eV]	$E_{\text{LUMO}}^{\text{c)}$ [eV]
IDIC-2F	722	791	1.57	-5.75	-3.95
MO-IDIC-2F	735	800	1.55	-5.80	-3.93
HO-IDIC-2F	739	798	1.55	-5.81	-3.91
DO-IDIC-2F	744	806	1.54	-5.79	-3.88

<sup>a)</sup>Absorption of the films; <sup>b)</sup>Calculated from the absorption edge of the polymer films:  $E_g^{\text{opt}} = 1240/\lambda_{\text{edge}}$ ; <sup>c)</sup>Calculated according to the equation  $E_{\text{LUMO/HOMO}} = -e(\varphi_{\text{red/ox}} + 4.36)$  (eV).

electrode, as shown in Figure S8 (Supporting Information) and the results are listed in Table 1. The SMAs exhibit similar highest occupied molecular orbital energy level ( $E_{\text{HOMO}}$ ), while the lowest unoccupied molecular orbital energy level ( $E_{\text{LUMO}}$ ) of the molecules up-shifted with the increase of alkoxy chains lengths, from -3.95 eV for IDIC-2F to -3.88 eV for DO-IDIC-2F (Table 1).

### 4. Single Crystal Structures and Charge Transport Properties of the SMAs

Solid state ordering of organic semiconductor molecules has significant effect on the intermolecular interactions.<sup>[32,33]</sup> Analyzing the single-crystal packing of n-type organic semiconductor acceptors is conducive to understanding the relationship between molecular structure, self-assembly and their charge transport properties.<sup>[34,35]</sup> However, few related studies have been reported, especially for the studies of the effect of alkyl chain changes on molecular self-assembly. In order to gain insight into the effect of alkyl chains on molecular accumulation, single-crystals of IDIC-2F, MO-IDIC-2F, HO-IDIC-2F, and DO-IDIC-2F were grown via slow evaporation of solvents, then the diffraction data were acquired.

The single-crystal structures of IDIC-2F, MO-IDIC-2F, HO-IDIC-2F, and DO-IDIC-2F are shown in Figure 2. From the crystal structures, we can observe that the alkoxy chain substituents extend along the molecular short axis. In addition, all these molecules exhibit the intramolecular  $\text{S}\cdots\text{O}=\text{C}$  interaction, which may provide an interlocking structure to fix the molecular conformation. In these molecules, the torsions between the electron pushing cores and the electron pulling end groups are observed. The IDIC-2F exhibits the largest torsions of 19.84°, while the torsions decreased to 12.18° in MO-IDIC-2F, 9.03° in HO-IDIC-2F, and 10.09° in DO-IDIC-2F. Furthermore, the differences in length of alkoxy chains also lead to dramatic differences in intermolecular packing. As shown in Figure 2b, IDIC-2F exhibits the brickwork arrangement with two kinds of  $\pi\cdots\pi$  interactions between neighbor molecules, the intermolecular  $\pi\cdots\pi$  distances are 3.46 and 3.72 Å, respectively. For MO-IDIC, the layered stacking of molecules mainly contains two kinds of interactions,  $\pi\cdots\pi$  interaction and  $\text{CN}\cdots\text{H}$  hydrogen bonding interaction, with distances of 3.61 and 2.38 Å, respectively. In addition, MO-IDIC-2F shows a J-aggregation via intermolecular  $\pi\cdots\pi$  stacking and piles into parallel arrangement along the molecular short axis direction (Figure 2d). In HO-IDIC-2F, substantial  $\pi\cdots\pi$  interactions between the electron

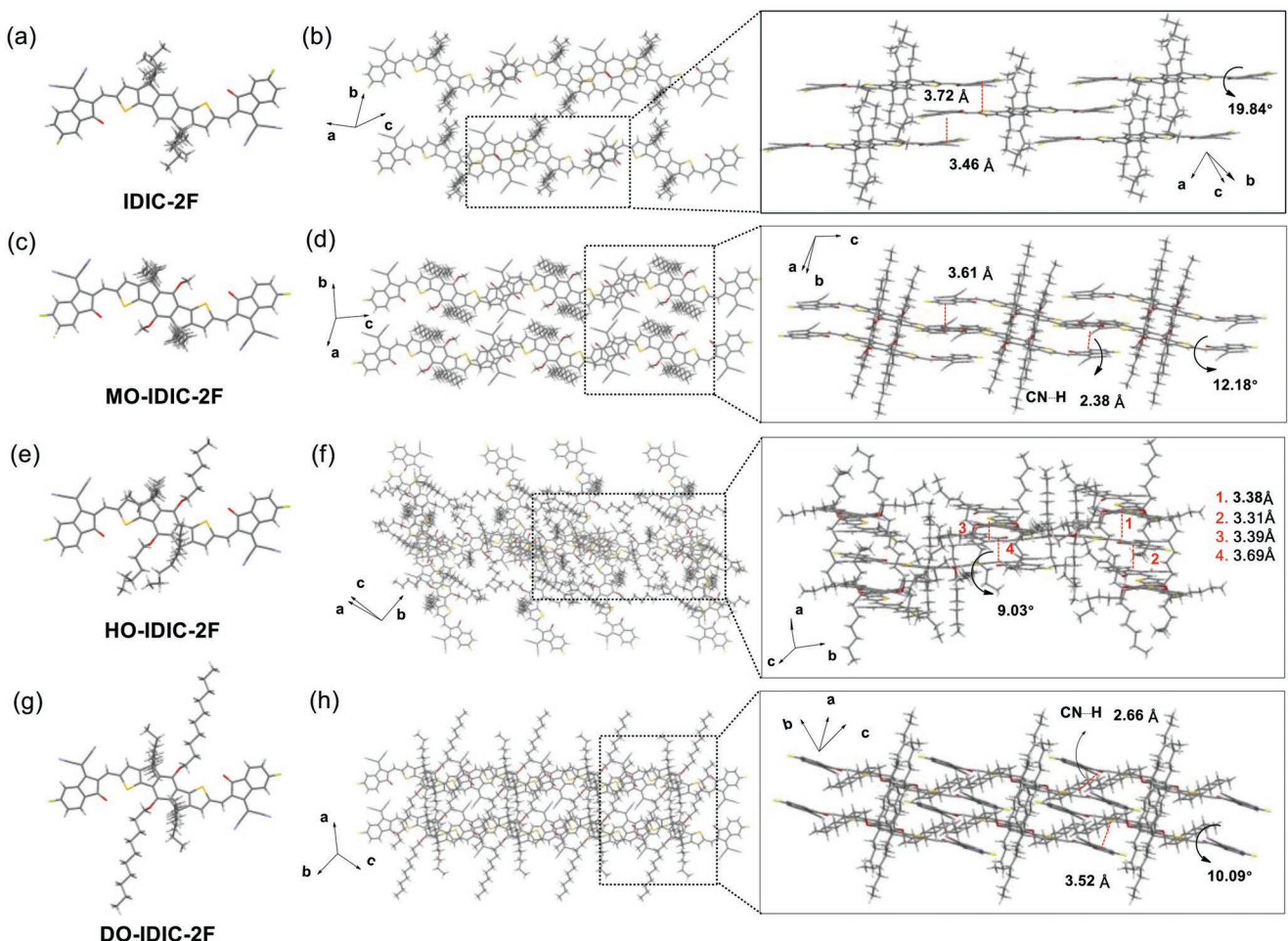


**Figure 2.** Single-crystal structures of a) IDIC-2F, c) MO-IDIC-2F, e) HO-IDIC-2F, and g) DO-IDIC-2F. Crystal packing structures of b) IDIC-2F, d) MO-IDIC-2F, f) HO-IDIC-2F, and h) DO-IDIC-2F.

pulling end groups with the distances of 3.38, 3.31, 3.39, and 3.69 Å are observed (Figure 2f), which promote the molecules to form a 3D network, which may be conducive to increase its charge transport properties. Note that DO-IDIC-2F adopts a packing similar to that of MO-IDIC-2F, the  $\pi$ - $\pi$  interactions between the electron pulling end groups with the spacing of  $\approx$ 3.52 and 2.66 Å CN···H is observed between neighboring DO-IDIC-2F molecules. However, owing to that the attached long alkoxy side chains prevent close approach of the neighboring molecules, DO-IDIC-2F exhibits *J*-aggregation in both of the  $\pi$ - $\pi$  interaction direction and molecular short axis direction (Figure 2h). It has been reported that *J*-aggregation is beneficial to exciton diffusion,<sup>[36]</sup> thus compared to MO-IDIC-2F, the aggregation of DO-IDIC-2F may be conducive to charge separation in materials.

The charge transfer integral plays a key role in determining the charge transport properties of organic molecules.<sup>[37]</sup> For these SMAs, the computed intermolecular interaction energies as well as electron transfer integrals ( $t_e$ ) were further investigated utilizing a series of systematically cropped dimer pairs, which further highlights the crucial role of the alkoxy side chains substitution on the electron transport properties. First,

select a molecule in the crystal lattice as the reference. Next the LUMO and LUMO(+1) orbital pairs of the dimers formation between the reference molecule and the nearest neighboring molecules are calculated (Figure 3a and Figures S9–S17, Supporting Information). Then  $t_e$  is approximately estimated by half of the energy splitting between the LUMO and LUMO(+1) dimer orbital pair (Figure 3b). The crystal structure of IDIC-2F contains two independent neighbors with the  $t_e$  of 38.5 and 36.2 meV. MO-IDIC-2F exhibits  $t_e$  of 78.4 meV from the intermolecular  $\pi$ - $\pi$  interaction, which is twice of that of IDIC-2F. HO-IDIC-2F have complex crystal structure. The different stacking patterns lead to significant differences in  $t_e$ , of which the largest  $t_e$  value is 79.7 meV and the lowest one is only 5.0 meV. Note that the charge transfer integrals of DO-IDIC-2F exhibit relatively small than that of other SMAs, which may be attributed to that the large alkoxy side chains prevent the effective interaction between adjacent molecules. Therefore, small variations in the intermolecular displacements within the dimers comprising the stacks will lead to significant changes in the magnitude of charge transfer integrals.

GIWAXS<sup>[38]</sup> was further used to investigate the molecular packing and the crystallinity of IDIC-2F, MO-IDIC-2F,

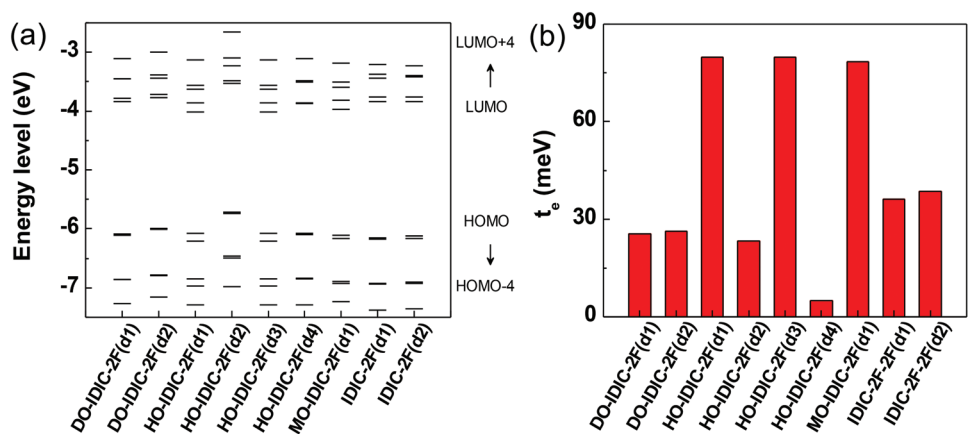


**Figure 3.** a) The calculated HOMO and LUMO orbital pairs of the acceptor dimers. b) Calculated electron transfer integrals ( $t_e$ ) of the acceptors based on the crystal packing.

HO-IDIC-2F, and DO-IDIC-2F in neat films. We prepared these SMAs thin films on Si substrates by spin-coating from their chloroform solutions. **Figure 4** displays the 2D GIWAXS patterns of the corresponding SMAs films and their line cuts in the in-plane and out-of-plane directions. All the neat materials show face-on orientation with  $\pi$ - $\pi$  stacking in the out-of-plane direction at about  $1.83 \text{ \AA}^{-1}$  and a sharp (100) reflection in the in-plane direction at about  $0.38 \text{ \AA}^{-1}$ . In the out-of-plane direction (Figure 4e), the  $\pi$ - $\pi$  stacking distances and the coherence lengths of IDIC-2F, MO-IDIC-2F, HO-IDIC-2F, and DO-IDIC-2F films are comparable, with a distance of 3.45, 3.41, 3.43, and 3.45  $\text{\AA}$ , and corresponding crystal coherence lengths of 64, 55, 63, and 64  $\text{\AA}$ , respectively. The GIWAXS results of the

SMAs films are consistent with the results of the single crystal analysis, which reveals that the side chain length has little effect on the  $\pi$ - $\pi$  stacking distance in these SMAs. In addition, these SMAs exhibit a high degree of molecular order, as evidenced by strong lamellar (100), (200) in the in-plane direction (Figure 4f). The position of the (h00) peaks are shifting to lower  $q$  when incrementing the side-chain length of the SMAs, which imply that the longer the side chain of SMAs, the larger the lamellar stacking distance of the molecules. More importantly, compared to IDIC-2F, the (100) peaks of other SMAs are narrower and the intensity is higher, which indicates the improved molecular ordering in films. Thus, the introduction of appropriate length alkoxy chains can effectively regulate the  $\pi$ - $\pi$

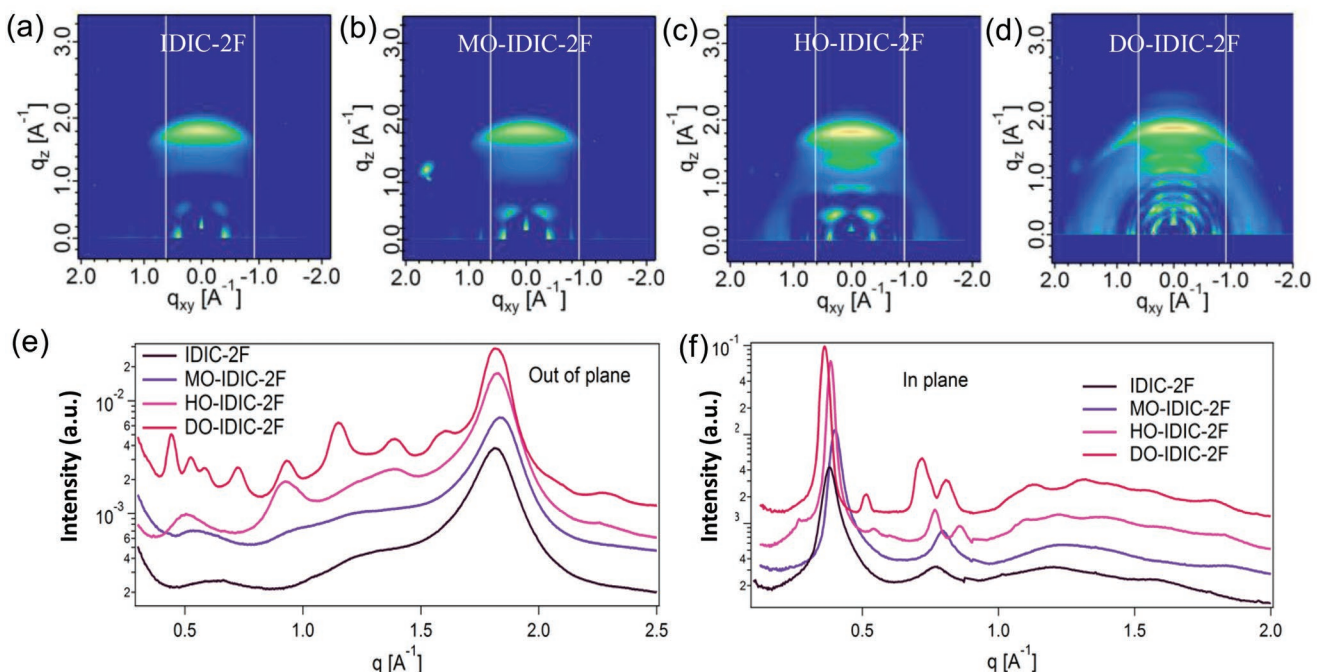


**Figure 4.** 2D GIWAXS patterns of a) IDIC-2F film, b) MO-IDIC-2F film, c) HO-IDIC-2F film and d) DO-IDIC-2F film; Line cuts of the GIWAXS of IDIC-2F, MO-IDIC-2F, HO-IDIC-2F, and DO-IDIC-2F films in e) out of plane direction and f) in plane direction. Line plots offset for clarity.

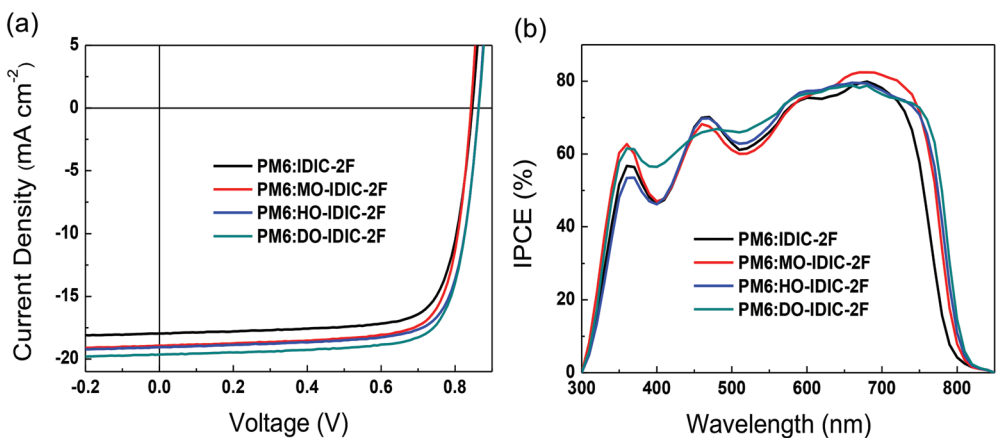


**Figure 5.** a)  $J$ - $V$  curves of the optimized PSCs based on PM6: acceptors (1:1, w/w) with thermal annealing at 120 °C for 5 min under the illumination of AM 1.5G, 100 mW cm<sup>-2</sup>; b) IPCE spectra of the corresponding PSCs.

stacking and improve the ordering of molecules in the films. The improved  $\pi$ - $\pi$  stacking and molecular ordering properties should be related to the  $J$ -aggregation of the SMAs mentioned above. The results indicate that the alkoxy side chains in the molecular short axis direction mainly lead to the difference in long-range ordering in the molecular aggregation, and the increase of the alkoxy chains in HO-IDIC-2F and DO-IDIC-2F result in complicated packing model which may improve the molecular ordering in films. This phenomenon is also consistent with the increased corresponding crystal coherence lengths and higher intensity (100) peaks of these SMAs in neat films.

In order to investigate the effect of the side chain length and different aggregation behavior of these SMAs on charge transport properties, the electron mobilities of the SMAs were measured using the space charge limited current (SCLC) method in electron-only devices with a structure of ITO/ZnO/active layer/PDINO/Al, as shown in Figure S18 (Supporting Information). The calculated electron mobilities are  $6.18 \times 10^{-4}$ ,  $8.94 \times 10^{-4}$ ,  $1.06 \times 10^{-3}$  and  $1.05 \times 10^{-3}$  cm<sup>2</sup> V<sup>-1</sup> s<sup>-1</sup> for IDIC-2F, MO-IDIC-2F, HO-IDIC-2F and DO-IDIC-2F respectively. The increased electron transfer integrals ( $t_e$ ) and improved molecular ordering from IDIC-2F to HO-IDIC-2F would be the reason for the gradually increased electron mobilities of these SMAs. For DO-IDIC-2F, the long alkoxy side chains prevent close approach of the neighboring molecules and decrease the corresponding  $t_e$ , which cooperates with the orderly accumulation of molecules lead to the similar electron mobilities of DO-IDIC-2F to HO-IDIC-2F.

## 5. Photovoltaic Performance

To understand the effect of side chain length on the photovoltaic performance of the SMAs, we fabricated the SMA-based PSCs with PM6 as donor, using the device configuration of glass/ITO/PEDOT:PSS/PM6:acceptors/PDINO/Al. Chloroform is used as the processing solvent and the optimized device fabrication conditions are: donor/acceptor weight ratio of 1:1, active layer thickness of  $\approx$ 110 nm and annealing temperature of 120 °C (see Tables S1 and S2 in the Supporting Information).

Figure 5 shows the current density–voltage ( $J$ - $V$ ) curves of the optimized PSCs based on PM6: acceptors under AM 1.5G simulated solar irradiation at 100 mW cm<sup>-2</sup> and the IPCE curves of the corresponding devices, and Table 2 lists the corresponding photovoltaic parameters for a clear comparison. Interestingly, the PCE values of the PSCs show a linear growth trend with the increase of alkoxy chains length of the acceptors, from 11.52% for IDIC-2F, to 12.23% for MO-IDIC-2F, 12.53% for HO-IDIC-2F, and 13.02% for DO-IDIC-2F. The  $V_{oc}$  of the devices have a slight increase from 0.846 V (IDIC-2F) to 0.864 V (DO-IDIC-2F), as a result of the up-shifted LUMO levels of the SMAs. The FF of the PSCs increased obviously from IDIC-2F to MO-IDIC-2F, while the continuous increase of the alkoxy chain length has little effect on FF for HO-IDIC-2F and DO-IDIC-2F. The  $J_{sc}$  values increased gradually with the increase of alkoxy chains length of the acceptors. For example, the IDIC-2F-based device afforded a relative lower  $J_{sc}$  value of 17.95 mA cm<sup>-2</sup>, whereas the DO-IDIC-2F-based device yielded a much higher  $J_{sc}$  value of 19.63 mA cm<sup>-2</sup>. The IPCE spectra of

**Table 2.** Photovoltaic Performance Parameters of the PSCs Based on PM6: acceptors under the illumination of AM1.5G, 100 mW cm<sup>-2</sup>.

Acceptor	$V_{oc}$ [V]	$J_{sc}$ [mA cm <sup>-2</sup> ]	FF [%]	PCE <sup>a</sup> [%]	$J_{sc}$ from IPCE [mA cm <sup>-2</sup> ]
IDIC-2F	0.846 (0.848 ± 0.007) <sup>b</sup>	17.95 (17.64 ± 0.25)	75.8 (75.5 ± 0.4)	11.52 (11.35 ± 0.23)	17.35
MO-IDIC-2F	0.843 (0.843 ± 0.005)	18.92 (18.21 ± 0.63)	76.7 (76.4 ± 0.7)	12.23 (12.21 ± 0.16)	18.26
HO-IDIC-2F	0.863 (0.860 ± 0.003)	19.05 (19.13 ± 0.31)	76.3 (76.2 ± 0.5)	12.53 (12.24 ± 0.33)	18.35
DO-IDIC-2F	0.864 (0.860 ± 0.004)	19.63 (19.47 ± 0.28)	76.5 (75.8 ± 1.2)	13.02 (12.94 ± 0.19)	18.79

<sup>a</sup>With thermal annealing at 120 °C for 5 min; <sup>b</sup>The values are calculated from more than 10 devices.

the corresponding devices (Figure 5b) supported the increasing  $J_{sc}$  values of the PSCs with the order of IDIC-2F, MO-IDIC-2F, HO-IDIC-2F, and DO-IDIC-2F.

To probe the exciton/charge dynamics, we measured the photocurrent density ( $J_{ph}$ ) dependence on the effective voltage ( $V_{eff}$ ) of the optimized devices, as shown in Figure S19a (Supporting Information). The  $J_{ph}$  values reach saturation ( $J_{sat}$ ) at 2 V, suggesting all the charges are collected by the electrodes. The charge dissociation probability can be calculated from  $J_{ph}/J_{sat}$ , which are 0.965, 0.966, 0.971, and 0.974 for the PSCs with IDIC-2F, MO-IDIC-2F, HO-IDIC-2F, and DO-IDIC-2F as acceptor respectively, implying the overall exciton dissociation and charge collection processes all are quite efficient for these PSCs.<sup>[39]</sup> We also measured the  $J_{sc}$  versus light density ( $P$ ) curves to study charge recombination behavior (Figure S19b, Supporting Information). The relationship between  $J_{sc}$  and  $P$  can be described as  $J_{sc} \propto P^\alpha$ . While  $\alpha < 1$  means the existence

of bimolecular charge recombination and  $\alpha = 1$  indicates there is no bimolecular charge recombination.<sup>[40]</sup> The  $\alpha$  values of the PSCs with IDIC-2F, MO-IDIC-2F, HO-IDIC-2F, and DO-IDIC-2F as acceptor are all above 0.96 (see Figure S19b in the Supporting Information), indicating that the bimolecular charge recombination are similar and weak in these PSCs.

## 6. Morphology Analysis

In order to gain a deeper understanding about the effect of the alkoxy chain length of the acceptors on the device performance, we conducted GIWAXS measurements on the blend films of the acceptors with PM6 as donor. As shown in Figure 6, all blend films show predominantly face-on orientation. In the in-plane direction line cut of the blend films (Figure 6f), shows that closer lamellar stacking in HO-IDIC-2F and DO-IDIC-2F is maintained

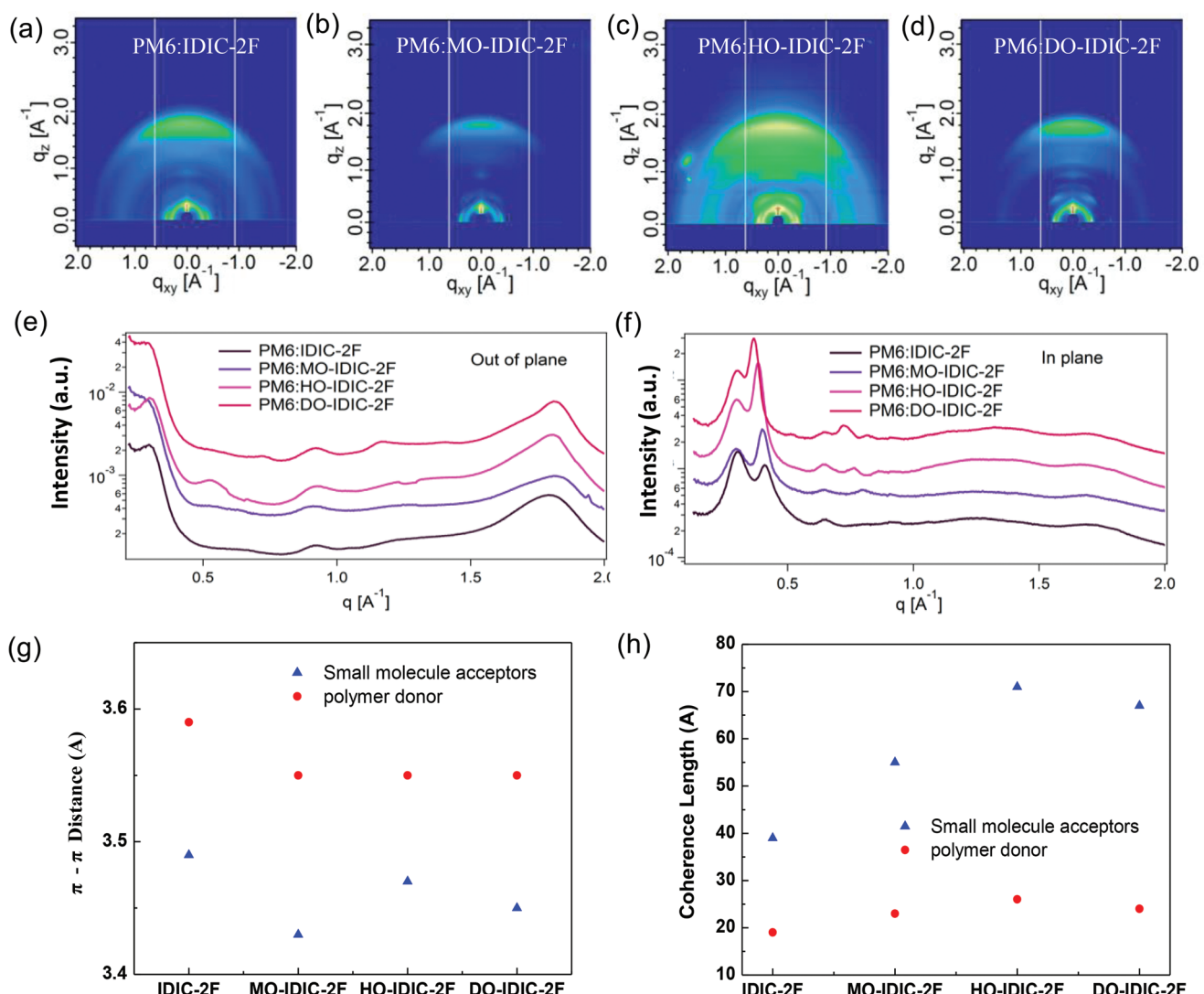


**Figure 6.** 2D GIWAXS patterns of a) PM6:IDIC-2F blend films, b) PBDB-T-2F:MO-IDIC-2F blend films, c) PM6:HO-IDIC-2F blend films, d) PM6:DO-IDIC-2F blend films. e) Line cuts of GIWAXS of the PM6:acceptors blend films in out of plane direction. f) Line cuts of GIWAXS of the PBDB-T-2F:acceptors blend films in in plane direction. g) The  $\pi - \pi$  distance in PM6:acceptors blend films. h) The  $\pi - \pi$  coherence length of PM6: acceptors blend films.

even in the blends. In the out-of-plane direction (Figure 6e), the  $\pi-\pi$  stacking peaks are similar across all the blends. However, the  $\pi-\pi$  coherence length of the SMAs increased significantly with the increase of alkoxy chain length (Figure 6h). The SMAs  $\pi-\pi$  peak coherence length is larger in the HO-IDIC-2F (71 Å) and DO-IDIC-2F (67 Å) blends as compared to the IDIC-2F blend (39 Å). The increase in the coherence length in DO-IDIC-2F and HO-IDIC-2F blends indicates improved molecular ordering, may attributed to the changes of the molecular accumulation, which is generally beneficial for charge transport (charge carrier mobilities are shown in Table S3 in the Supporting Information) in vertical direction as well as for reducing charge recombination and hence helps improve the PCE of the devices.

The surface and bulk morphology of PM6: acceptors blend films were studied by atomic force microscopy (AFM) and transmission electron microscopy (TEM), as shown in Figure S20 in the Supporting Information. The films exhibit a uniform and smooth surface with a relatively small root-mean-square (RMS) roughness of 1.26, 1.29, 1.26, and 1.17 nm for the IDIC-2F, MO-IDIC-2F, HO-IDIC-2F, and DO-IDIC-2F blend films respectively. In the TEM images, the blend films exhibit finely dispersed phase separation, which is consistent with the morphology observed by AFM.

## 7. Conclusion

Two new small molecule acceptors HO-IDIC-2F and DO-IDIC-2F were synthesized for investigating the effect of the alkoxy side chain lengths on the physicochemical, self-assembly and photovoltaic properties of the acceptors, together with the other two acceptors of IDIC-2F and MO-IDIC-2F. In the film, from IDIC-2F to DO-IDIC-2F, the absorption spectra red-shifted and the lowest unoccupied molecular orbital up-shifted gradually with the increase of alkoxy chains length. The single-crystal structure analysis and GIWAXS results indicate that alkoxy side chain length influences the molecular self-assembly of the acceptors significantly. The single-crystal analysis reveals that the longer side chains have little effect on the  $\pi-\pi$  stacking distances in these SMAs, however, can promote HO-IDIC-2F to form a 3D network and DO-IDIC-2F to form J-aggregation in both of the  $\pi-\pi$  interaction direction and molecular short axis direction. In addition, with the increasing of alkoxy chains length from IDIC-2F to DO-IDIC-2F, the (100) peaks of these SMAs are narrowed, indicating the improved molecular order in their films. These characteristics of molecular packing could be the intrinsic reason for the gradually increased charge transport properties of the SMAs. The GIWAXS experiments further provide the insight on the changes in the morphology of photoactive layers based on these SMAs. The improved molecular order, of the SMAs in blend films with the increase of alkoxy chains length in the SMAs can explain the enhanced photovoltaic performance of the PSCs with the acceptors from IDIC-2F (11.52%) to DO-IDIC-2F (13.02%). Thus, we illuminated that the side chains length plays an important role on the molecular self-assembly, morphology and photovoltaic performance of the PSCs, and the side chain engineering of SMAs provides an effective way to regulate the properties of SMAs and further improve the photovoltaic performance of the PSCs.

## Supporting Information

Supporting Information is available from the Wiley Online Library or from the author.

## Acknowledgements

X.L., H.H., and I.A. contributed equally to this work. This work was financially supported by NSFC (Nos. 91633301, 51820105003, and 21734008) and the Strategic Priority Research Program of the Chinese Academy of Sciences, Grant No. XDB12030200. NCSU gratefully acknowledges the support of ONR grant N000141712204. X-ray data were acquired at beamline 7.3.3 at the Advanced Light Source, which is supported by the Director, Office of Science, Office of Basic Energy Sciences, of the U.S. Department of Energy under Contract No. DE-AC02-05CH11231. C.Z. and A. Hexemer of the ALS (LBNL) provided support and instrument maintenance.

## Conflict of Interest

The authors declare no conflict of interest.

## Keywords

molecular self-assembly, morphology, polymer solar cells, side chain engineering, small molecule acceptors

Received: August 20, 2019

Revised: September 25, 2019

Published online: October 24, 2019

- [1] R. Søndergaard, M. Hösel, D. Angmo, T. T. Larsen-Olsen, F. C. Krebs, *Mater. Today* **2012**, *15*, 36.
- [2] J. Hou, O. Inganäs, R. H. Friend, F. Gao, *Nat. Mater.* **2018**, *17*, 119.
- [3] C. J. Traverse, R. Pandey, M. C. Barr, R. R. Lunt, *Nat. Energy* **2017**, *2*, 849.
- [4] G. Li, R. Zhu, Y. Yang, *Nat. Photonics* **2012**, *6*, 153.
- [5] B. Kan, Q. Zhang, M. Li, X. Wan, W. Ni, G. Long, Y. Wang, X. Yang, H. Feng, Y. Chen, *J. Am. Chem. Soc.* **2014**, *136*, 15529.
- [6] Y. Liu, J. Zhao, Z. Li, C. Mu, W. Ma, H. Hu, K. Jiang, H. Lin, H. Ade, H. Yan, *Nat. Commun.* **2014**, *5*, 5293.
- [7] H. Bin, Z. G. Zhang, L. Gao, S. Chen, L. Zhong, L. Xue, C. Yang, Y. F. Li, *J. Am. Chem. Soc.* **2016**, *138*, 4657.
- [8] Z. He, C. Zhong, S. Su, M. Xu, H. Wu, Y. Cao, *Nat. Photonics* **2012**, *6*, 591.
- [9] J. Yuan, Y. Zhang, L. Zhou, G. Zhang, H.-L. Yip, T.-K. Lau, X. Lu, C. Zhu, H. Peng, P. A. Johnson, M. Leclerc, Y. Cao, J. Ulanski, Y. F. Li, Y. Zou, *Joule* **2019**, *3*, 1140.
- [10] S. Zhang, Y. Qin, J. Zhu, J. Hou, *Adv. Mater.* **2018**, *30*, 1800868.
- [11] S. Dey, *Small* **2019**, *15*, 1900134.
- [12] H. Sun, F. Chen, Z.-K. Chen, *Mater. Today* **2019**, *24*, 94.
- [13] W. Zhao, S. Li, H. Yao, S. Zhang, Y. Zhang, B. Yang, J. Hou, *J. Am. Chem. Soc.* **2017**, *139*, 7148.
- [14] N. Qiu, H. Zhang, X. Wan, C. Li, X. Ke, H. Feng, B. Kan, H. Zhang, Q. Zhang, Y. Lu, Y. Chen, *Adv. Mater.* **2017**, *29*, 1604964.
- [15] S. Dai, F. Zhao, Q. Zhang, T. K. Lau, T. Li, K. Liu, Q. Ling, C. Wang, X. Lu, W. You, X. Zhan, *J. Am. Chem. Soc.* **2017**, *139*, 1336.
- [16] Z. Yao, X. Liao, K. Gao, F. Lin, X. Xu, X. Shi, L. Zuo, F. Liu, Y. Chen, A. K. Jen, *J. Am. Chem. Soc.* **2018**, *140*, 2054.
- [17] W. Liu, J. Zhang, Z. Zhou, D. Zhang, Y. Zhang, S. Xu, X. Zhu, *Adv. Mater.* **2018**, *30*, 1800403.

- [18] X. Shi, L. Zuo, S. B. Jo, K. Gao, F. Lin, F. Liu, A. K. Y. Jen, *Chem. Mater.* **2017**, *29*, 8369.
- [19] S. Feng, C. Zhang, Y. Liu, Z. Bi, Z. Zhang, X. Xu, W. Ma, Z. Bo, *Adv. Mater.* **2017**, *29*, 1703527.
- [20] Y. Li, N. Zheng, L. Yu, S. Wen, C. Gao, M. Sun, R. Yang, *Adv. Mater.* **2019**, *31*, 1807832.
- [21] T. J. Aldrich, S. M. Swick, F. S. Melkonyan, T. J. Marks, *Chem. Mater.* **2017**, *29*, 10294.
- [22] J.-D. Lin, L. Zhong, F.-P. Wu, Y. Li, Y. Yuan, H. Bin, Z. Zhang, F. Liu, J. Fan, Z.-G. Zhang, L.-S. Liao, Z.-Q. Jiang, Y. Li, *Sci. China: Chem.* **2018**, *61*, 1405.
- [23] W. Gao, Q. An, R. Ming, D. Xie, K. Wu, Z. Luo, Y. Zou, F. Zhang, C. Yang, *Adv. Funct. Mater.* **2017**, *27*, 1702194.
- [24] W. Gao, T. Liu, R. Ming, Z. Luo, K. Wu, L. Zhang, J. Xin, D. Xie, G. Zhang, W. Ma, H. Yan, C. Yang, *Adv. Funct. Mater.* **2018**, *28*, 1803128.
- [25] T. Liu, W. Gao, Y. Wang, T. Yang, R. Ma, G. Zhang, C. Zhong, W. Ma, H. Yan, C. Yang, *Adv. Funct. Mater.* **2019**, *29*, 1902155.
- [26] Z. Fei, F. D. Eisner, X. Jiao, M. Azzouzi, J. A. Rohr, Y. Han, M. Shahid, A. S. R. Chesman, C. D. Easton, C. R. McNeill, T. D. Anthopoulos, J. Nelson, M. Heeney, *Adv. Mater.* **2018**, *30*, 1705209.
- [27] Y. Yang, Z. G. Zhang, H. Bin, S. Chen, L. Gao, L. Xue, C. Yang, Y. F. Li, *J. Am. Chem. Soc.* **2016**, *138*, 15011.
- [28] X. Li, H. Huang, Z. Peng, C. Sun, D. Yang, J. Zhou, A. Liebman-Pelaez, C. Zhu, Z.-G. Zhang, Z. Zhang, Z. Xie, H. Ade, Y. F. Li, *J. Mater. Chem. A* **2018**, *6*, 15933.
- [29] X. Li, F. Pan, C. Sun, M. Zhang, Z. Wang, J. Du, J. Wang, M. Xiao, L. Xue, Z. G. Zhang, C. Zhang, F. Liu, Y. F. Li, *Nat. Commun.* **2019**, *10*, 519.
- [30] L. Ye, W. Li, X. Guo, M. Zhang, H. Ade, *Chem. Mater.* **2019**, *31*, 6568.
- [31] C. Zhang, W. Wang, W. Huang, J. Wang, Z. Hu, Z. Lin, T. Yang, F. Lin, Y. Xing, J. Bai, H. Sun, Y. Liang, *Chem. Mater.* **2019**, *31*, 3025.
- [32] M. Mas-Torrent, C. Rovira, *Chem. Rev.* **2011**, *111*, 4833.
- [33] P. M. Beaujuge, J. M. Frechet, *J. Am. Chem. Soc.* **2011**, *133*, 20009.
- [34] T. J. Aldrich, M. Matta, W. Zhu, S. M. Swick, C. L. Stern, G. C. Schatz, A. Facchetti, F. S. Melkonyan, T. J. Marks, *J. Am. Chem. Soc.* **2019**, *141*, 3274.
- [35] M. Polkehn, H. Tamura, P. Eisenbrandt, S. Haacke, S. Mery, I. Burghardt, *J. Phys. Chem. Lett.* **2016**, *7*, 1327.
- [36] T. Y. Li, J. Benduhn, Z. Qiao, Y. Liu, Y. Li, R. Shrivhare, F. Jaiser, P. Wang, J. Ma, O. Zeika, D. Neher, S. C. B. Mannsfeld, Z. Ma, K. Vandewal, K. Leo, *J. Phys. Chem. Lett.* **2019**, *10*, 2684.
- [37] J. Calvo-Castro, M. Warzecha, A. R. Kennedy, C. J. McHugh, A. J. McLean, *Cryst. Growth Des.* **2014**, *14*, 4849.
- [38] A. Hexemer, W. Bras, J. Glossinger, E. Schaible, E. Gann, R. Kirian, A. MacDowell, M. Church, B. Rude, H. Padmore, *J. Phys.: Conf. Ser.* **2010**, *247*, 012007.
- [39] Y. Yang, Z. Zhang, H. Bin, S. Chen, L. Gao, L. Xue, C. Yang, Y. F. Li, *J. Am. Chem. Soc.* **2016**, *138*, 15011.
- [40] P. Schilinsky, C. Waldauf, C. Brabec, *Appl. Phys. Lett.* **2002**, *81*, 3885.